4760–4773 *Nucleic Acids Research, 2023, Vol. 51, No. 10* *Published online 13 March 2023*
https://doi.org/10.1093/nar/gkad146

Symmetric control of sister chromatid cohesion establishment

Jiaxin Zhang[1,†], Lili Li[1,†], Yu Miao[2], Xiaojing Liu[1], Haitao Sun[1], Meiqian Jiang[1], Xiaoli Li[1], Zhen Li[3], Cong Liu[4], Baohua Liu[1], Xingzhi Xu[1], Qinhong Cao[1], Wenya Hou[1,5], Chunlai Chen[2] and Huiqiang Lou[1,*]

[1]Guangdong Key Laboratory for Biomedical Measurements and Ultrasound Imaging, School of Biomedical Engineering, Guangdong Key Laboratory for Genome Stability & Disease Prevention, School of Basic Medical Sciences, Shenzhen University Medical School, South China Hospital, Shenzhen 518116. State Key Laboratory of Agrobiotechnology, College of Biological Sciences, China Agricultural University, Beijing 100193, China, [2]School of Life Sciences; Beijing Advanced Innovation Center for Structural Biology; Beijing Frontier Research Center of Biological Structure, Tsinghua University, Beijing 100084, China, [3]State Key Laboratory of Plant Physiology and Biochemistry, College of Biological Sciences, China Agricultural University, Beijing 100193, China, [4]Department of Paediatrics, SCU-CUHK Joint Laboratory for Reproductive Medicine, Key Laboratory of Birth Defects and Related Diseases of Women and Children (Ministry of Education), West China Second University Hospital, Sichuan University, 610041 Chengdu, China and [5]Shenzhen University General Hospital and School of Medicine, Guangdong Key Laboratory for Genome Stability & Disease Prevention, School of Basic Medical Sciences, Shenzhen University Medical School, Shenzhen University, Shenzhen 518060, China

Received August 17, 2022; Revised February 13, 2023; Editorial Decision February 15, 2023; Accepted February 19, 2023

ABSTRACT

Besides entrapping sister chromatids, cohesin drives other high-order chromosomal structural dynamics like looping, compartmentalization and condensation. ESCO2 acetylates a subset of cohesin so that cohesion must be established and only be established between nascent sister chromatids. How this process is precisely achieved remains unknown. Here, we report that GSK3 family kinases provide higher hierarchical control through an ESCO2 regulator, CRL4^{MMS22L}. GSK3s phosphorylate Thr105 in MMS22L, resulting in homo-dimerization of CRL4^{MMS22L} and ESCO2 during S phase as evidenced by single-molecule spectroscopy and several biochemical approaches. A single phospho-mimicking mutation on MMS22L (T105D) is sufficient to mediate their dimerization and rescue the cohesion defects caused by GSK3 or MMS22L depletion, whereas non-phosphorylable T105A exerts dominant-negative effects even in wildtype cells. Through cell fractionation and time-course measurements, we show that GSK3s facilitate the timely chromatin association of MMS22L and ESCO2 and subsequently SMC3 acetylation. The necessity of ESCO2 dimerization implicates symmetric control of cohesion establishment in eukaryotes.

INTRODUCTION

Sister chromatid cohesion is a crucial determinant of chromosome integrity as it facilitates the accurate flow of genetic material to daughter cells via faithful chromosome segregation (1). This process is mediated by cohesin, a highly conserved multi-subunit protein complex in eukaryotes. It is composed of four core subunits: SMC1, SMC3, RAD21 (Scc1 in yeast), and either SA1 or SA2 (Scc3 in yeast), which together forms a ring-like structure encircling DNA (2–4). Besides entrapping sister chromatids, cohesin also drives high-order structural changes that include chromatin looping, compartmentalization and condensation (5,6). Therefore, cohesin must be precisely regulated by numerous accessory factors in time and space to execute the proper functions (7–10).

Cohesin can be loaded onto chromatin throughout the large portion of the cell cycle and often retains a highly dynamic state of association. A stable cohesion state is established by ESCO2 or ESCO1 (EStablishment of COhesion, Eco1/Ctf7 in yeast) that acetylates the cohesin subunit SMC3 and thereby counteracts the anti-establishment activity of WAPL (Rad61 in yeast) (11–16). ESCO2-catalyzed SMC3 acetylation must be strictly controlled to guaran-

*To whom correspondence should be addressed. Tel: +86 0755 86930275; Fax: +86 0755 86930275; Email: lou@szu.edu.cn
†The authors wish it to be known that, in their opinion, the first two authors should be regarded as Joint First Authors.

tee that cohesion must be established and only established between nascent sister chromatids. Besides the S-phase-specific expression, ESCO2/Eco1 is directly coupled with the moving replication fork through physical interactions with several fork components like MCM, PCNA and $CRL4^{MMS22L}$ in yeast and humans (17–23).

While some aspects of the exquisite regulation of ESCO2 have come to light, it remains largely unknown why ESCO2 is not targeted to the excessive cohesin complexes that spread throughout the chromatin during S phase. We hypothesize that a higher hierarchical system might be needed to present ESCO2 exclusively to cohesin that holds sister chromatids. Through screening new proteins interacting with the known ESCO2 regulators, we have identified that GSK3 family kinases provide more stringent spatial-temporal control of ESCO2-catalyzed SMC3 acetylation through $CRL4^{MMS22L}$. GSK3A/B (yeast Mck1), isolated initially as Glycogen Synthase Kinase 3, phosphorylate Thr105 in MMS22L (Thr127 in yeast Mms22), mediating homo-dimerization of both $CRL4^{MMS22L}$ and ESCO2 exclusively in S phase. A single phospho-mimicking mutation of MMS22L (*mms22L*-T105D) is sufficient to mediate its self-interaction and bypass the role of GSK3s in cohesion. Through cell fractionation and time-course measurements, we show that GSK3s facilitate the efficient association of MMS22L and ESCO2 onto chromatin and subsequently promote SMC3 acetylation in S phase. The unanticipated requirements of ESCO2 homo-dimerization implicate a 2-fold symmetric pattern of cohesion establishment between nascent sister chromatids in both yeast and human cells.

MATERIALS AND METHODS

Cell culture, transfection, strains

HeLa, HEK293T and HepG2 cell lines were grown in a humidified 5% CO2 incubator at 37°C in DMEM (Gibco) supplemented with 10% FBS (ABW) and standard antibiotics. 293F cells were cultured in SMM 293-TI (Sino Biological) media supplemented with 1% FBS, 100 U/ml penicillin and 100 mg/ml streptomycin.

For transient transfection, 1×10^6 cells were seeded per 100 mm dish for 12 h prior to the delivery of plasmid DNA or siRNA using Lipofectamine 3000 (Invitrogen).

The *Saccharomyces cerevisiae* strains used in this study were listed in Supplementary Table S1.

Cloning and DNA manipulations

RaPure Total RNA kit (Magen) was used to isolate total RNA according to the manufacturer's instructions. cDNA was synthesized using reverse transcriptase (Promega). CUL4A, CUL4B, DDB1, MMS22L and ESCO2 plasmids for transient expression were generated previously (22). GSK3A and GSK3B full-length genes were generated by PCR and were inserted into the pRK5-FLAG vector. All genes were sub-cloned into other vectors when necessary. See Supplementary Table S2 for details of plasmids used in this study, Supplementary Table S3 for plasmids generated in this study, and Supplementary Table S4 for primers used in this study.

Table 1. The sequences of siRNA oligo

Target gene	Sequences of siRNA oligo
GSK3A	5'-GAAGGUUCUCCAGGACAAG-3'
GSK3B	5'-AGUUAGCAGAGACAAGGAC-3'
GSK3A&B	5'-AUCUUUGGAGCCACUGAUU-3'
MMS22L	5'-UCACAAAGUCCUUGGAAUA-3'
	5'-AAGACUUGCUGUUGCGAUA-3'
NC	5'-UUCUCCGAACGUGUCACGU-3'

Generation of GSK3-knockout cells

Knockout Cell lines were generated using CRISPR-Cas9 (24). Briefly, two guide sequences targeting two different sites of the target gene were inserted into the pX330 vector. The pX330 plasmids expressing gRNA were transfected into HEK293T cells. Single colonies were picked after 8–10 days of incubation and validated by sequencing and Western blotting.

RNA interference (RNAi)

For RNAi experiments, cells were transfected with siRNAs using Lipofectamine 3000 (Invitrogen) for 48 h following the manufacturer's instructions. Immunoblotting with specific antibodies was used to confirm the downregulation of the targets. The sequences of siRNA used in this study are listed in Table 1. All siRNAs were synthesized by Sangon Biotech, China.

Cell synchronization and drug treatments

HeLa or HEK293T cells were synchronized in early S phase using double-thymidine blocks, 14–16 h in the presence of 2 mM thymidine (Sigma), 8–10 h release, and 16 h in the presence of 2 mM thymidine. And the synchronized cells were collected at the indicated time points after the second release. For the enrichment of cells in prometaphase, 100 ng/ml nocodazole (Sigma) was added 5 h after release from the second thymidine block, and mitotic cells were collected by the shake-off method. For the arrest of cells in G2 phase, 10 μM RO-3306 (Selleckchem) was added 4.5 h after release from the second thymidine block.

HepG2 cells were synchronized in early G1/S phase by 0.4 mM mimosine (Sigma) treatment for 24 h. The synchronized cells were washed with DPBS three times, released and collected at the indicated time points after release.

The GSK3 kinase inhibitor CHIR-98014 was purchased from Selleckchem. For GSK3i treatment, 5 μM CHIR-980145 was applied for 12 h unless otherwise indicated.

Chromosome spreads

Chromosome spreads were performed as previously described (25) with minor modifications. In brief, HEK293T cells were grown asynchronously after siRNA transfection. Mitotic cells were collected by trypsinization and hypotonically swollen in 75 mM KCl for 5 min at room temperature. Cells were fixed twice with Carnoy's solution (methanol: acetic acid; 3:1) and then dropped onto glass slides. Chromosomes were stained with 10% [v/v] Giemsa (Amresco), washed with water, and air-dried. Images were captured at

RT using a Leica CytoVision microscope equipped with 100×/NA1.3 oil objective.

Yeast sister chromatid cohesion assays

Sister chromatid cohesion assays were performed as previously described (26). Yeast strains (kind gifts provided by Dr. Sue Biggins at Fred Hutchinson Cancer Research Center) were grown overnight at 30°C in YPDA. Cells were diluted to 2.5 × 10^6 cells/ml in fresh YPDA media containing 25 μM $CuSO_4$. The cultures were grown at 30°C for 3 h and then released in fresh YPDA media supplemented with 15 μg/ml nocodazole to synchronize cells in M phase. Harvested cells were fixed in 100 μl of paraformaldehyde at room temperature for 15 min, washed with SK buffer (1 M $KHPO_4$, 50 mM sorbitol). Samples were observed at RT using a Leica DMI8 microscope equipped with 100×/NA1.4 oil objective, Leica DFC 9000 GTC camera, and Leica Application Suite X software.

Flow cytometry cell cycle analysis

Synchronized HEK293, HepG2 or yeast cells were collected by trypsinization and fixed in 70% ethanol overnight at −20°C. After washing with PBS twice, cell pellets were re-suspended in PBS containing 10 μg/ml propidium iodide and 500 μg/ml ribonuclease A for 30 min at room temperature. Flow cytometry was performed with a CytoFLEX S flow cytometer (Beckman coulter). Data analysis was performed using Kaluza Analysis software.

Immunoprecipitation

Cells were collected, washed with PBS twice, and lysed on ice for 30 min in the lysis buffer (50 mM Tris–HCl, 150 mM NaCl, 1% [v/v] NP-40, 5 mM EDTA, 10% [v/v] glycerin) followed by sonication. After removal of the insoluble fraction by centrifugation at 16 100 × *g* for 15 min, the remainder of each cell extract was used for immunoprecipitation. Anti-FLAG M2 (Sigma) beads were added to cell extract containing 300 μg total protein and incubated at 4°C for 2 h in a rotating wheel. After being washed four times with the lysis buffer, the bound proteins were boiled in the loading buffer and subjected to western blot analysis using the indicated antibodies.

Glutaraldehyde (GA)-crosslinking assays

Glutaraldehyde (GA) crosslinking was used to detect the MMS22L dimer *in vivo*. Briefly, HEK293T cells transiently transfected with the indicated MMS22L mutants were washed with ice-cold PBS and lysed in the lysis buffer (20 mM HEPES, 150 mM NaCl, 1% [v/v] NP-40, 5 mM EDTA, 10% [v/v] glycerin). Cell lysates (25 μg total protein) were incubated with 0.02% glutaraldehyde (Merck) for 30 min on ice. The reaction was quenched by incubation with 50 mM Tris–HCl (pH7.5) for 15 min. Then, the samples were boiled and used for western blot assays.

Gel filtration

Analytical gel-filtration studies were conducted with Superdex 200 Increase 10/300 column on an ÄKTA FPLC (GE Healthcare) at 4°C. To investigate the interaction between Eco1 and Mms22, a 1:1 (molar ratio) mixture of Eco1:Mms22 in lysis buffer (50 mM Tris–HCl, 150 mM NaCl) was injected. The protein sample was eluted at a 0.25 ml/min flow rate with lysis buffer, and fractions of 0.5 ml each were collected using an automatic fraction collector (GE Healthcare). Proteins in each fraction were analyzed by SDS-PAGE and immunoblotting.

Chromatin fractionation analysis

This analysis was performed as described previously with slight modifications (27). Whole-cell extract (WCE) and supernatant (SN) samples were taken from the same batch of samples used for chromatin fractionation. Cells harvested from 60 mm dishes were re-suspended in CSK buffer (300 mM sucrose, 0.1 M NaCl, 10 mM PIPES, pH 7.0, 0.5% Triton X-100, 1 mM $MgCl_2$, 1 mM EDTA, 2 mM PMSF, 10 mM NaF, 20 mM β-glycerophosphate, 100 μM Na_3VO_4) and incubated on ice for 20 min. Chromatin and non-chromatin fractionation were separated by centrifugation at 2000 × *g* for 15 min at 4°C. The insoluble pellet, including chromatin, was washed with CSK buffer and centrifuged again. The pellet re-suspended in the CSK buffer is referred to as the chromatin fraction.

Fluorescence polarization measurements

For *in vitro* polarization measurements, FITC-labeled MMS22L T^{105} peptide, FITC-labeled pT^{105} peptide, or MMS22L protein was diluted to a final concentration of 10 ng/μl in the MMS22L lysis buffer in a final volume of 100 μl. The mixture was incubated and measured in a black/clear 96-well plate (BD Falcon), using a SPARK microplate reader (TECAN) equipped with a fluorescence polarization filter, excitation at 485 nm and emission at 535 nm. Polarization was calculated using SparkControl analysis software (TECAN) according to the following equation:

$$FP = [(I_{\parallel} - G \times I_{\perp})/(I_{\parallel} + G \times I_{\perp})]$$

The *G* factor (compensation factor for the plate reader) was set automatically for each measurement based on gain adjustment settings. The sequence of peptides used in this study is as follows:

- MMS22L T^{105}: FITC-YNLETLLQSSCD
- MMS22L pT^{105}: FITC-YNLE (pT) LLQSSCD

Biomolecular fluorescence complementation assay (BiFC)

HEK293T cells were seeded at a density of 1 × 10^5 cells per well onto coverslips in six-well plates. Plasmids expressing GFP-N-ESCO2, GFP-C-ESCO2, GFP-N or GFP-C were incubated with Lipofectamine 3000 (Invitrogen) and transiently transfected into cells 48 h post-transfection. After being fixed with 4% paraformaldehyde, cells were then stained with DAPI for 5 min, mounted, and visualized at

RT by Leica DIM8 confocal microscopy equipped with 40×/NA0.85 air objective or 100×/NA1.4 oil objective, a Leica DFC 9000 GTC camera, Leica Application Suite X software. Synchronization and drug treatment are performed as described above.

Fluorescence correlation spectroscopy (FCS) and photon counting distribution (PCD) assays

FCS and PCD measurements were performed with the home-built confocal microscopy. Light from the excitation source (OBIS 488 nm LS 100 mW Laser) passes sequentially through a non-contact receptacle style fiber collimator (OZ OPTICS HPUCO-23AF-400/700-*P*-6AC-15) and an absorptive ND filter (THORLABS NE20B) and is finally piped into the objective (Zeiss Plan-APOCHORMAT 100×/1.4 Oil DC) mounted on the prototyping inverted microscope (Zeiss Apo Observer D1). The backscattered fluorescence from the excited specimen is collected with the same objective. To eliminate the after-pulse effect, passing through a 50 μm pinhole (THORLABS P50HW), the signal was split (THORLABS CM1-BS013) into two avalanche photodiode detectors (APDs, Excelitas SPCM-AQRH-14) in front of which bandpass filters (Chroma ET525/50m) are equipped to separate the emission signal from the excitation light. The active region of the APD features a diameter of 180 μm, capable to be its own pinhole.

The yeast cells were grown to a logarithmic phase at 30°C in an SC medium and arrested in G1 by 2.5 μM α-factor. After G1 arrest, cells were released in the same fresh medium supplemented with 2% galactose. 100 OD_{600} units of cells were collected at the indicated time points. Cells were lysed by glass bead beating (3970 rpm, 6.5 m/s, 1 min on, 1 min off, 10 cycles, 4°C) in lysis buffer (50 mM HEPES, pH7.5, 150 mM NaCl, protease inhibitor).

PEG-passivation alleviates protein non-specific absorption onto the slides and the preparation procedure followed the previously reported protocol (28,29). To acquire reasonable PCD curves, each cell lysate was diluted (50 mM HEPES pH7.5, 150 mM NaCl) to a concentration corresponding to 2–4 molecules detected in the confocal spot where GFP should emit at the intensity of 25–50 kHz excited by the 488 nm laser at 10 mW. The photon arrival time from two separated APDs was recorded for 10 s and fed to a digital correlator (Flex02-01D/C) synchronously calculating intensity trace and FCS curves. We employed a home-developed MATLAB program to output the PCD at any manually selected bin time. 10 repeats were carried out for each sample. Global analysis of FCS and PCD was accomplished with the software FFS Data Processor 2.7 (30).

Protein purification and *in vitro* kinase assays

293F cells expressing FLAG-tagged MMS22L, GSK3A or GSK3B were washed with PBS twice and lysed in the lysis buffer. Proteins were purified by anti-FLAG M2 beads (Sigma) and washed three times in washing buffer (50 mM Tris–HCl, 500 mM NaCl, 1% [v/v] NP-40, 5% [v/v] glycerin, 2 mM PMSF, 10 mM NaF, 20 mM β-glycerophosphate, 100 μM Na_3VO_4). Proteins were then eluted in the lysis buffer supplemented with 2 mg/ml FLAG peptide. The eluent components were collected and stored in aliquots at -80°C before use.

FLAG-tagged Mck1 was purified from BY4741 yeast strain. The pRS313-pADH1-*MCK1-5FLAG* plasmid was transformed into an *mck1*Δ strain. 200 OD_{600} units of logarithmic cells were lysed by glass bead beating (Mini-Beadbeater-16, Biospec) in the lysis buffer (50 mM Tris–HCl, pH7.5, 500 mM NaCl, 1% [v/v] NP-40, 10% [v/v] glycerin, 2 mM PMSF, 10 mM NaF, 20 mM β-glycerophosphate, 100 μM Na_3VO_4). Mck1 was purified by anti-FLAG M2 beads (Sigma) and eluted by 1 mg/ml FLAG peptide.

BL21-codon-plus (DE3)-RIL *E. coli* strain (Stratagene) was transformed with pET vectors expressing His × 6-FLAG-Mms22N or His × 6-Eco1. The expression was induced at $OD_{600} = 0.6$ with 0.02 mM IPTG at 25°C for 3 h. The protein was purified using Ni^{2+}-beads (GE Healthcare) and eluted with 500 mM imidazole.

Antibodies

Antibodies used in this work were as below: anti-GSK3 α/β (CST, #5676), anti-ESCO2 (Abcam, ab86003), anti-MMS22L (Abcam, ab181047), anti-SMC3 (BETHYL, A300-060A), anti-acetyl SMC3 Lys105/106 (Merck, MABE1073), anti-ORC2 (CST, #4736), anti-Tubulin (MBL, PM054), anti-FLAG (Sigma, F3165), anti-Myc (Proteintech, 16286-1-AP), anti-mCherry (Proteintech, 26765–1-AP). To raise polyclonal antibodies specific to Eco1, purified full-length protein was used to immunize rabbits.

Statistical analysis

GraphPad Prism v8.3 was used to graph data and statistical analyses. All data shown in the histograms are the results of at least three independent experiments and are presented as the mean ± SEM. Data distribution was assumed to be normal, but this was not formally tested. ANOVA, two-tailed Student's *t*-test, or multiple *t*-tests were performed as appropriate to compare means. Statistical tests used are specified in the figure legends. Statistical significance was determined at the level of n.s., $P > 0.05$; *$P < 0.05$; **$P < 0.01$; ***$P < 0.001$; ****$P < 0.0001$.

RESULTS

GSK3 kinases play a conserved role in sister chromatid cohesion

To investigate the mechanism through which the cohesion reaction occurs exclusively in the context of nascent sister chromatids, we set out to identify new interaction partners of the known ESCO2 regulators using yeast two-hybrid screens. Yeast GSK3 family kinase, Mck1, caught our attention because it showed positive interaction with Mms22 (Supplementary Figure S1A), the substrate adaptor of $CRL4^{Mms22}$ jointly linking Eco1-catalyzed Smc3 acetylation with DNA replication (22,23). Their human orthologues, GSK3A and MMS22L, also interacted with each other (Supplementary Figure S1B), suggesting that GSK3-MMS22L interaction might be highly conserved.

We next asked whether GSK3 participates in sister chromatid cohesion as $CRL4^{MMS22L}$. To test this, we measured the cohesion efficiency in human HEK293T cells. GSK3A or GSK3B was knocked down using siRNA. Chromosome morphology was analyzed through chromosome spreading and Giemsa staining of the mitotic shake-off cells. Cohesion phenotypes were classified into four categories (Figure 1A): closed (i), the entire sister chromatids are closely paired with each other; arms open (ii), sister chromatid arms are splayed apart or have bubbles; railroad (iii), sister chromatids are separated but still paired; unpaired (iv), every chromatid is completely separated from its sister. We calculated the percentages of severe cohesion defects as the proportion of 'iii and iv' cells among total mitotic cells. Depletion of either GSK3A or GSK3B had no apparent effect on cohesion (Figure 1B). However, simultaneous depletion of GSK3A and GSK3B caused an approximately 15% loss of cohesion (Figure 1B), close to the extent in MMS22L-depleted cells reported previously (Supplementary Figure S1C) (22,23). This indicates that human GSK3A and GSK3B play a redundant role in cohesion. To confirm this result, we applied CRISPR-Cas9 gene editing in HEK293T cell line to generate GSK3 knockout clones. Again, $GSK3A^{-/-}$ or $GSK3B^{-/-}$ cells had no apparent cohesion defects (Figure 1C). However, we could not obtain the GSK3A and GSK3B double-knockout cells after many attempts, presumably due to synthetic lethality (31,32). To overcome this barrier, we treated cells with CHIR-98014 (GSK3i), a specific inhibitor of both GSK3A and GSK3B kinases, and noticed an additional ∼15% loss of cohesion as well (Figure 1D). These results indicate that GSK3A and GSK3B make a substantial contribution to sister chromatid cohesion in human cells.

In parallel, we assessed the cohesion status in yeast cells containing 256 *lac* operator (*lacO*) repeats integrated at several different chromosomal locations. This specific chromosome locus was then recognized and labeled by GFP-tagged LacI (GFP-LacI) protein (26). Exponentially growing cells were arrested in metaphase by nocodazole and examined by fluorescent microscopy. A single GFP spot indicates proper cohesion of two intimately tethered sister chromatids, whereas two GFP spots reflect precocious sister chromatid separation (Figure 1E). At telomeres, ∼18% of *mck1*Δ cells exhibited two GFP foci, and reintroduction of a plasmid expressing Mck1 rescued the cohesion deficiency to a near wild type (WT) level (∼7%) (Figure 1F). Consistently, premature loss of cohesion was observed at centromeres and chromosomal arms as well (Figure 1G, H; Supplementary Figure S1D). Moreover, *mck1*Δ*mms22*Δ displayed a similar cohesion defect as either single mutant (Figure 1G; Supplementary Figure S1D, E), indicating an epistatic genetic interaction between *MCK1* and *MMS22*. Yeast or human cells defective in both PCNA- and $CRL4^{MMS22L}$- mediated Eco1/ESCO2 recruitment pathways show an additive loss of SMC3 acetylation, sister chromatid cohesion and cell viability (22,23). Like *mms22*Δ, *mck1*Δ was also synthetic lethal at low temperatures (<25°C) with a cold-sensitive Eco1-interacting defective *PCNA* allele (*pol30*-A251V) (Supplementary Figure S1F). Taken together, these results corroborate that GSK3s are involved in sister chromatid cohesion in both yeast and human cells as their putative partner, MMS22L.

MMS22L is a substrate of GSK3 kinases

We next sought to determine the molecular mechanism by which GSK3s regulate sister chromatid cohesion. Given the possible interaction between GSK3 and Mms22, we tested whether Mms22 is a substrate of GSK3 kinases. In vitro kinase assay was performed using purified recombinant Mms22 protein fragments and GSK3s in the presence of γ-^{32}P-ATP. Consistent with previous studies (33–35), purified GSK3A or Mck1 kinase alone displayed auto-phosphorylation (Figure 2A, lanes 2, 3, 6 and 7). Among the truncations, only Mms22 N-terminus (a.a. 1–300, Mms22N) was phosphorylated by either yeast Mck1 or human GSK3 kinases (Figure 2A, lanes 6–8). GSK3B, with undetectable auto-phosphorylation activity (lane 4), could phosphorylate Mms22N, though to a less extent than GSK3A (compare lanes 7–8). To exclude the possibility that Mms22N was phosphorylated by the contaminant kinase(s) copurified with GSK3, we adopted two strategies. First, we added GSK3i to the *in vitro* reactions. GSK3i potently inhibited auto-phosphorylation of GSK3A as well as phosphorylation of Mms22N by both GSK3A and GSK3B (Figure 2A, compare lanes 15–16 to 7–8). Notably, GSK3i could hardly inhibit yeast Mck1-catalyzed auto-phosphorylation and Mms22N phosphorylation as well (Figure 2A, compare lanes 14 to 6). Second, Mms22N was hardly phosphorylated by *mck1*-KD (kinase-defective, D164A) (Figure 2B, lane 11). With the kinase specificity validated, these data indicate that Mms22 is a direct substrate of GSK3 family kinases.

To identify the phosphorylation sites of Mms22 by GSK3, we partially purified endogenous FLAG-tagged Mms22 protein from yeast cells by FLAG-immunoprecipitation (IP) and analyzed by LC-MS/MS. Mass spectra revealed that S126 or T127 of Mms22 are potential phosphorylation sites (Supplementary Figure S2A–C). According to the consensus sites (S/T-X-X-X-S/T(p)) recognized by all GSK3 family kinases (36), Mms22 S131 and S126/T127 might be the prime site and phosphorylation sites, respectively. Indeed, compared with Mms22N WT, *mms22N*-3A (S126A, T127A and S131A) showed a significant decrease whereas *mms22N*-S131D (a mutant mimicking primed phosphorylation) had an increase in phosphorylation by Mck1 (Figure 2B, lanes 6–8). By contrast, *mms22N*-S131D was barely targeted by *mck1*-KD (lane 11). These data verify that Mms22 S126/T127 are the bona fide phosphorylation sites of Mck1. Moreover, T127 remains invariable from yeast to human (MMS22L T105) (Supplementary Figure S2D), suggesting that Mms22 T127 (MMS22L T105) is a conserved GSK3 phosphorylation site.

$CRL4^{MMS22L}$ forms homo-dimers in an S-phase-specific manner

What is the consequence of GSK3-dependent Mms22 phosphorylation? Our first postulation was that Mms22 phosphorylation might affect its protein-protein interactions. The self-interaction of Mms22 identified in the yeast two-hybrid screen caught our attention (Supplementary Figure S2E). To confirm this, we performed three experiments

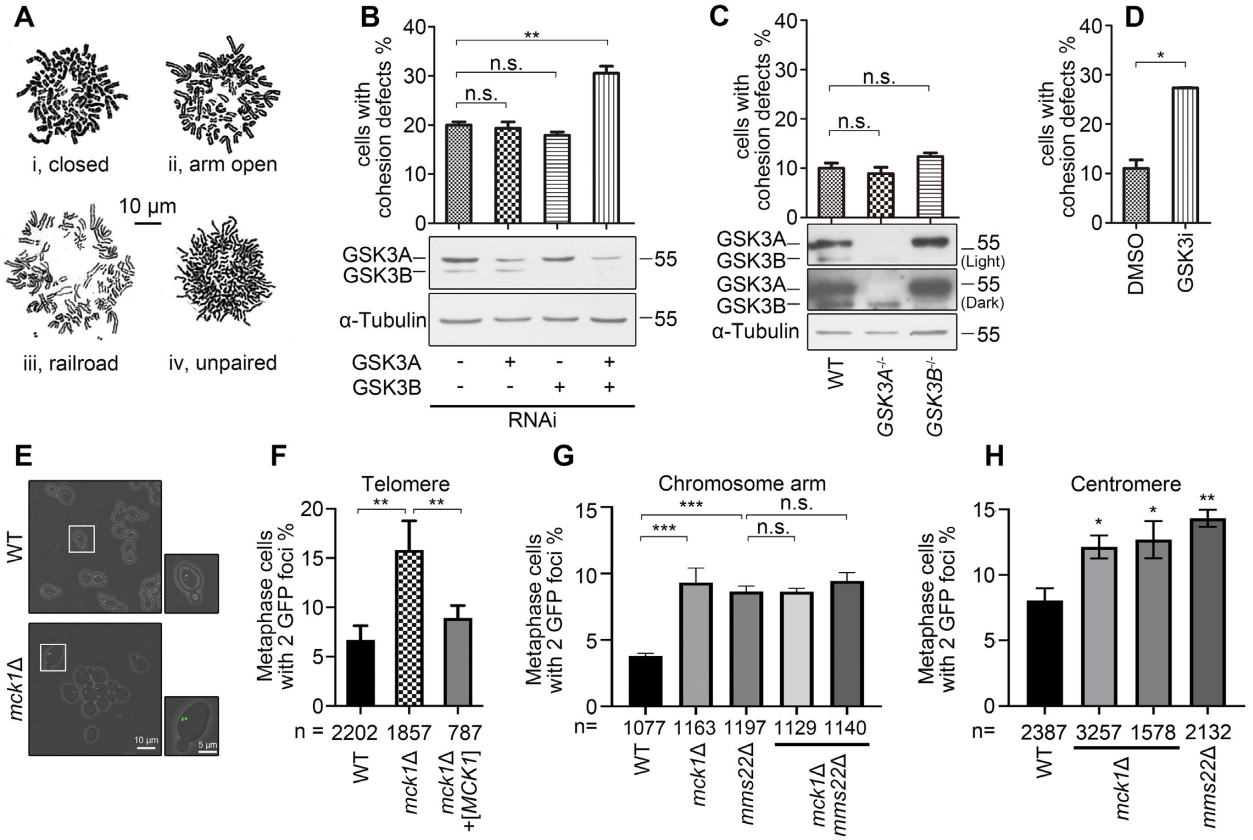

Figure 1. GSK3 family kinases are required for sister chromatid cohesion in yeast and humans. (**A**) Representative images of different classes of chromosome morphology in chromosome spread analysis. Bar: 10 μm. (**B**) Quantification of cohesion defects with or without knockdown of GSK3s. Mitotic cells were harvested by shake-off and examined by chromosome spreading and Giemsa staining. At least 200 cells per RNAi experiment were classified into four categories. The percentage of cells with severe cohesion defects (railroad or unpaired) among the total mitotic cells was quantified from three independent biological repeats. Means ± SEM are shown. The statistical significance was calculated via the student's *t*-test, ** $P < 0.01$. The efficiency of siRNA was detected via immunoblots against the indicated antibodies. (**C**) Chromosome spread analysis of GSK3A or GSK3B knockout cell line. (**D**) Chromosome spread analysis of cells with or without GSK3i treatment. (**E**) Representative pictures of yeast cohesion assays in wild-type (SBY180) and *mck1*Δ cells. Bar: 10 μm (*left*), 5 μm (*right*). (F–H) *mck1* null mutant exhibits precocious sister chromatid separation at telomeres (SBY180 background, **F**), chromosome arms (SBY214 background, **G**) and centromeres (SBY885 background, **H**). Cells were grown to log phase and sequentially synchronized with α-factor and nocodazole. At least 200 metaphase-arrested cells were counted for each experiment. Means ± SEM are shown. The statistical significance was calculated via Student's *t*-test, * $P < 0.05$, ** $P < 0.01$, *** $P < 0.001$.

in human cells. First, we ectopically expressed FLAG-MMS22L and Myc-MMS22L in 293T cells and carried out FLAG-IP. Myc-MMS22L co-precipitated with FLAG-MMS22L (Figure 2C, lane 4), but not with untagged MMS22L (lane 3). Using the same strategy, we also detected the self-interactions of other subunits of $CRL4^{MMS22L}$, CUL4 and DDB1, in human cells (Supplementary Figure S2F, G), suggesting the existence of dimeric or oligomeric forms of $CRL4^{MMS22L}$ *in vivo*.

Second, to investigate whether the self-interaction of MMS22L is regulated during the cell cycle, we repeated FLAG-IP experiments using cells synchronized in different cell cycle stages. Post-double-thymidine blocks, early-S phase and middle-S phase cells were obtained by release for 0 and 4 h, respectively. G2/M and M phase cells were arrested by RO-3306 and nocodazole treatment, respectively. Comparable amounts of FLAG-MMS22L were precipitated from all cellular extracts; the amounts of Myc-MMS22L in the precipitates, however, fluctuated significantly throughout the cell cycle with a peak in S phase and a rapid decline in G2 (Figure 2D). These results imply that MMS22L likely interacts with itself in a cell-cycle-regulated pattern, correlating with the timing of cohesion establishment in S and cohesion dissolution in G2/M.

Third, we overexpressed FLAG-MMS22L in HEK293T cells and detected its oligomeric status by *in vivo* crosslinking with glutaraldehyde (GA). Without GA-crosslinking, only a ∼130 kDa-migrating FLAG-MMS22L species, equivalent to the monomeric form, was visible (Figure 2E). After GA-crosslinking, a prominent >250 kDa-migrating form of FLAG-MMS22L appeared concomitantly with a decline of MMS22L monomers. These data suggest the existence of MMS22L dimers *in vivo*, which can be captured by chemical crosslinking. We further examined the crosslinked MMS22L species in cells synchronized at different cell cycle stages. MMS22L dimers were barely detectable in G1 and became evident in S followed by a decline in G2/M (Supplementary Figure S2H), generally consistent with the cell cycle-dependent self-interaction shown in Figure 2D. Altogether, these data suggest that $CRL4^{MMS22L}$ may form

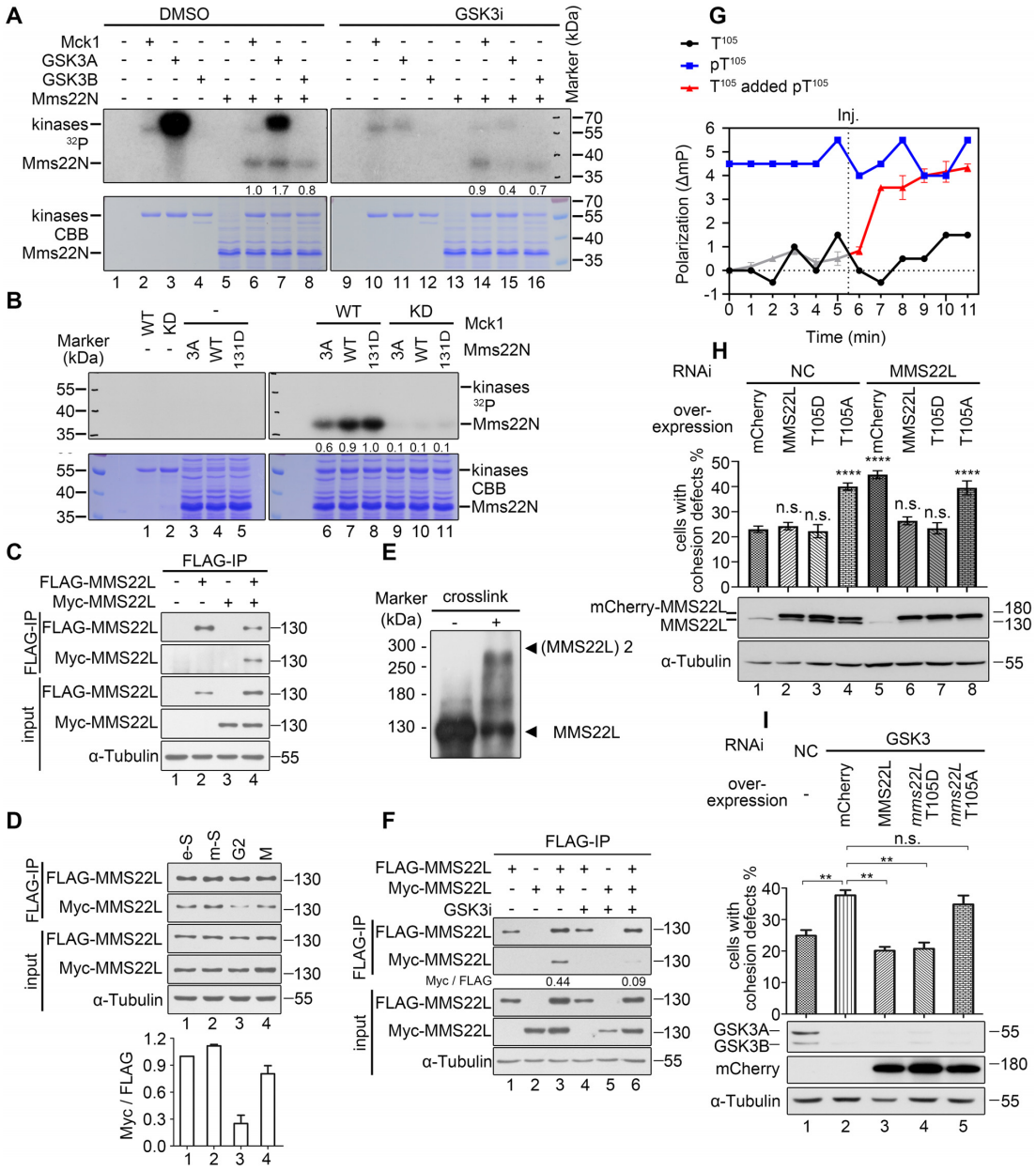

Figure 2. The cohesion role of GSK3s is solely attributed to phosphorylating MMS22L T105 and subsequently MMS22L dimerization. (A) Mms22 is a substrate of GSK3s (**A**) or yeast Mck1 (**B**). Recombinant Mms22 N-terminus (Mms22N, 1–300) was incubated with Mck1/GSK3 in the presence of γ-^{32}P-ATP. The samples were resolved by SDS-PAGE followed by autoradiography (*upper panel*). The loaded protein in each reaction was shown by Coomassie brilliant blue (CBB) (*lower panel*). *mck1*-KD (D164A), *mms22N*-S131D and *mms22N*-3A were applied as controls in the kinase assays. (**C**) MMS22L interacts with itself. HEK293T Cells were transfected for 2 days with expression constructs for the proteins indicated at the top of each panel. Cells were lysed and then subjected to immunoprecipitation (IP) with FLAG-M2 beads, as described in Materials and Methods. Immunoprecipitates and aliquots of the cell lysates were analyzed by western blotting with the indicated antibodies. (**D**) Self-interaction of MMS22L during the cell cycle. HEK293T cells expressing FLAG-MMS22L and Myc-MMS22L were cultured and synchronized in different cellular stages. FLAG-IP was carried out followed by western blotting (*left*). The representative immunoblots were shown. Band intensities from two independent experiments were quantified by Quantity One software. The relative ratio of Myc-MMS22L to FLAG-MMS22L in the precipitates was calculated (*right*). (**E**) MMS22L dimers detected by *in vivo* glutaraldehyde (GA) crosslinking. HEK293T cells expressing FLAG-MMS22L were treated with or without 0.02% GA, followed by Western blot analysis with an anti-FLAG antibody. (**F**) The self-interaction of MMS22L depends on GSK3. FLAG-IP was conducted as described in (C) using cells with or without GSK3i treatment. Band intensities were quantified by Quantity One software. (**G**) The fluorescence polarization assays for MMS22L FL and MMS22L peptide (a.a. 101–112) with or without phosphorylation at T^{105} (pT^{105} or T^{105}). The fluorescence polarization was measured and quantified from at least three independent biological samples with three technical replicates for each sample. In the competition experiments (grey/red curve), pT^{105} peptide was injected into the T^{105} peptide and MMS22L FL pre-mixture at the indicated time point. (**H**) Overexpression of *MMS22L*-T105D mutant suppresses the cohesion defects in the MMS22L-depleted cells. Means ± SEM are shown. The statistical significance was calculated via one-way ANOVA analysis, **** $P < 0.0001$. The efficiency of siRNA and overexpression of the genes were detected via immunoblots against the indicated antibodies. (**I**) Overexpression of *MMS22L*-T105D mutant suppresses the cohesion defects in the GSK3-depleted cells. Cohesion defects in the indicated HEK293T cells were analyzed as described in Figure 1B. Means ± SEM are shown. The statistical significance was calculated via the Student's *t*-test, ** $P < 0.01$. The efficiency of siRNA and overexpression of the genes were detected via immunoblots against the indicated antibodies.

dimers during S phase through direct dimerization between the substrate adaptor subunit MMS22L.

CRL4^{MMS22L} is dimerized through GSK3-dependent MMS22L T105 phosphorylation

We next examined whether MMS22L dimerization depends on GSK3-mediated MMS22L phosphorylation using four sets of experiments. First, we repeated the FLAG-IP experiments shown in Figure 2C with or without GSK3i treatment. The co-precipitated Myc-MMS22L was nearly abolished after GSK3i treatment (Figure 2F, compare lanes 6 to 3). Second, GSK3i also vastly reduced MMS22L dimers captured by GA-crosslinking (Supplementary Figure S2I, compare lanes 7 to 4). Third, compared to WT MMS22L or T105D mutant, T105A showed a compromised dimerization (Supplementary Figure S2I, lanes 1–3, 4–6). Importantly, unlike WT, T105D dimers became resistant to GSK3i (Supplementary Figure S2I, compare lanes 8 to 7), indicating a persistent dimerization of this phosphomimetic mutant protein. Fourth, we used fluorescence polarization assays to compare the direct binding between purified full-length human MMS22L protein and fluorescence FITC-labeled synthetic peptide of MMS22L (a.a. 101–112) with or without phosphorylation on T105 residue (pT105). As shown in Figure 2G, the pT105 peptide displayed significantly higher polarization than the T105 unmodified peptide. Further, we injected the equimolar pT105 peptide 5.5 min after pre-incubation of the T105 peptide with MMS22L and observed a sharp increase in polarization (Figure 2G, red curve). This reflects a potent competitive association of the pT105 peptide over the T105 peptide. Putting together, these data allow us to conclude that MMS22L dimerization is directly mediated through T105 phosphorylation by GSK3s.

GSK3-dependent MMS22L phosphorylation is critical for cohesion establishment

After establishing the critical role of T105 phosphorylation in MMS22L dimerization, we wanted to evaluate the contribution of this single residue modification to sister chromatid cohesion. Plasmids expressing various mCherry-*MMS22L* alleles were introduced into MMS22L-depleted cells. Chromosome spreading showed that overexpression of the phospho-mimetic form, *mms22L*-T105D, completely rescued precocious sister chromatid separation as overexpression of *MMS22L* WT (Figure 2H, compares lanes 5–7). On the contrary, overexpression of the unphosphorylated form, *mms22L*-T105A, had nearly no effect (lane 8), demonstrating an indispensable role of T105 phosphorylation for MMS22L in sister chromatid cohesion. Strikingly, when these *mms22L* alleles were introduced into HEK293T control cells, T105A overexpression was sufficient to cause a dramatic cohesion defect to a similar extent as MMS22L-depletion, whereas T105D and WT overexpression had no effect (Figure 2H, compares lanes 4–5). Such a potent dominant-negative effect of *mms22L*-T105A is in agreement with the role of T105 phosphorylation in mediating CRL4^{MMS22L} dimerization as shown above. Taken together, these data indicate that the role of MMS22L in sister chromatid cohesion relies on T105 phosphorylation-dependent CRL4^{MMS22L} dimerization.

We next reasoned that if MMS22L defines the major downstream target of GSK3s, reinforcement of MMS22L could compensate for the role of GSK3s in sister chromatid cohesion. To test this, we repeated the above genetic suppression assays in GSK3 knockdown human cells. T105D, but not T105A, could efficiently rescue their cohesion defects (Figure 2I, compared lanes 3–5 to Figure 2H lanes 6–8). Moreover, such distinct effects of the counterpart phospho-mutations were completely reproduced in WT and *mck1*Δ yeast cells (Supplementary Figure S2J). *MMS22L*/*MMS22* displayed a similar suppression effect as the phospho-mimicking mutants, presumably due to the high dosage-induced MMS22L dimerization. These data strongly indicate that the role of GSK3s in cohesion is solely attributed to MMS22L T105 phosphorylation and subsequent CRL4^{MMS22L} dimerization from yeast to humans.

GSK3 promotes self-interaction of ESCO2 during S phase

Given the fact that each Eco1/ESCO2 contains one Mms22-binding motif (LxG) (22,23), we next asked whether Mms22 dimers are able to recruit two ESCO2 molecules simultaneously. Although the physiological significance has not been addressed, yeast Eco1 interacts and acetylates itself as independently reported by the Nasmyth and Koshland groups (13,37). Schüler and his colleagues further show that human ESCO1 can exist as a dimer in solution (38). To test whether human ESCO2 can form dimers *in vivo*, we performed bimolecular fluorescence complementarity (BiFC) in HEK293T cells expressing two versions of ESCO2 with one carrying GFP N-terminus (GFP-N) and the other carrying GFP C-terminus (GFP-C). The GFP signal was only visible in the presence of both GFP-N-ESCO2 and GFP-C-ESCO2, implying possible self-interaction of ESCO2 (Figure 3A and Supplementary Figure S3A). To answer whether ESCO2 dimerization is cell-cycle-regulated, we examined it in the synchronized cells. Interestingly, the fluorescence was not detectable till the cells proceeded into S phase (Figure 3A, B, Supplementary Figure S3C). The fluorescence density peaked around 6–8 h after release from double-thymidine blocks, basically coincident with the timing of cohesin dimerization in 293T cells (39). These results suggest that two ESCO2 molecules might exist in proximity specifically during S phase. Notably, mms22L-T105A-mCherry overexpression abolished the ESCO2-BiFC signals, whereas overexpression of MMS22L or T105D had no effect (Supplementary Figure S3D). Congruent with its dominant negative effect in sister chromatid cohesion shown in Figure 2H, this indicates that the non-phosphorylated form of MMS22L interferes with both the proximity of ESCO2 molecules and sister chromatid cohesion. Consistently, the ESCO2-BiFC signals disappeared after GSK3i treatment (Figure 3C, D, Supplementary Figure 3B), which could be fully rescued by introducing mms22L-T105D, but not T105A (Figure 3E, F), indicating that T105 phosphorylation is sufficient to bypass GSK3 in triggering putative self-interaction of ESCO2. Together, these data suggest that GSK3-mediated

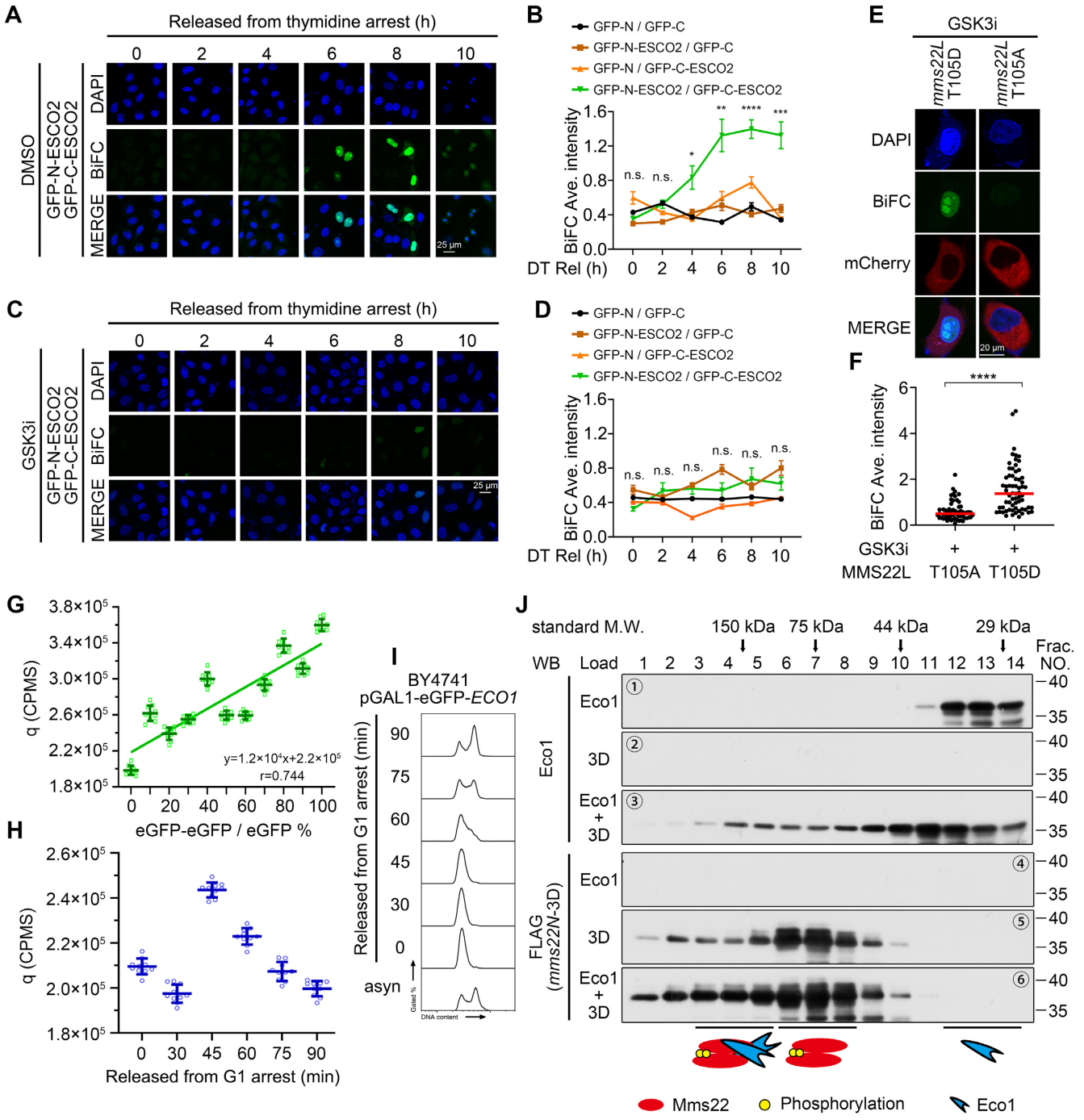

Figure 3. GSK3s promote self-interaction of ESCO2 during S phase. (**A**) Representative images of the BiFC assays of ESCO2. HEK293T cells carrying the indicated expression plasmids were synchronized using double-thymidine release (DT-Rel) and harvested at different time points for confocal microscopy. Scale bar, 25 μm. (**B**) The GFP fluorescence intensities of cells were quantified. At least ten fields were analyzed for each sample. The data represent mean ± SEM, $*P < 0.05$, $**P < 0.01$, $***P < 0.001$, $****P < 0.0001$. The statistical significance was calculated via two-way ANOVA analysis. (**C**) Representative images of ESCO2-BiFC assays after GSK3i treatment. Scale bar, 25 μm. (**D**) The GFP fluorescence intensities of cells treated with GSK3i were quantified. At least ten fields were analyzed for each sample. The data represent mean ± SEM. The statistical significance was calculated via two-way ANOVA analysis. (**E**) Representative images of ESCO2-BiFC assay in cells expressing *MMS22L*-T105D or *MMS22L*-T105A after GSK3i treatment. Scale bar, 20 μm. (**F**) The GFP fluorescence intensities of mCherry-positive cells were quantified. Cell samples were harvested at 8 h after DT-Rel. At least 50 mCherry-positive cells were analyzed from two individual experiments. Red bars represent the median. At least 50 tracts were scored for each sample. The statistical significance was calculated via the Student's *t*-test, $****P < 0.0001$. (**G**) The **q** standard curve of the indicated mixtures of eGFP and eGFP-eGFP by PCD analysis. (**H**, **I**) PCD analysis of cells expressing endogenous eGFP-Eco1 throughout the cell cycle. Cells were synchronized in G1 and released into S phase for the indicated time. The cell-cycle profiles were analyzed by flow cytometry (I). (**J**) Gel filtration analyses of the Eco1-Mms22N complex. Purified Eco1, *mms22N*-3D (S126, T127, S131D) or a mixture of Eco1 and *mms22N*-3D (1:1 molar ratio) was subjected to gel filtration with the indicated molecular standards. After separation, each fraction was detected via immunoblots against the indicated antibodies.

MMS22L homo-dimerization might recruit two ESCO2 molecules simultaneously during S phase.

To further validate this notion, we examined the Eco1 oligomerization status in yeast by single-molecule spectroscopy tools such as fluorescence correlation spectroscopy (FCS) and photon counting distribution (PCD). FCS can measure fluctuations in fluorescence intensity, which correlates with molecular diffusion through a sub-femtoliter volume. While PCD analysis can provide the true brightness per particle (q) from which the oligomerization status would be derived (40). A q standard curve was established using a serial mixture of mGFP (monomer) and mGFP-mGFP (tandem-dimer) with different ratios (Figure 3G). Yeast cells were synchronized in G1 before release for the indicated time. The cell lysates of each sample were then subjected to FCS and PCD analysis as described in Materials & Methods. GFP-Eco1 was only detectable as a monomer in G1 (Figure 3H). Near 20% GFP-Eco1 behaved as a dimer when cells proceeded into S phase for 45 min followed by a quick decline to 0% at ∼90 min (late S phase) (Figure 3H, I). These data suggest that a subset of Eco1 shows an S-phase-specific dimerization pattern as its substrate cohesin (39).

We next performed size exclusion chromatography to directly examine the oligomeric state of the Mms22-Eco1 complex reconstituted *in vitro*. Purified recombinant yeast His6-Eco1 (35 kDa) was detected in fractions 12–14, between the 29 and 44 kDa molecular standards, indicating that Eco1 alone exists as a monomer *in vitro* (Figure 3J, panel 1 and Supplementary Figure S3E). Meanwhile, mms22N-3D (S126, T127, S131D) (∼37 kDa) mostly presented in fractions 6–8 (∼75 kDa) (Figure 3J, panel 5 and Supplementary Figure S3E), consistent with its existence as a dimer *in vivo* as shown in Figure 2. Interestingly, after incubation with mms22N-3D, a small portion of Eco1 migrated in a complex with dimeric mms22N-3D to near ∼150 kDa positions concomitantly with a reduced amount of Eco1 in ∼35 kDa fractions (Figure 3J, panel 3 and Supplementary Figure S3E). These results implicate that Eco1 and mms22N-3D may form a 2:2 heterotetramer (∼145 kDa) *in vitro*. Putting all the above *in vitro* and *in vivo* observations together, we propose that Eco1/ESCO2 might act in a dimeric form mediated by GSK3-dependent MMS22L dimerization.

GSK3s-mediated dimerization of CRL4^{MMS22L} enhances SMC3 acetylation and thereby sister chromatid cohesion

Because the essential role of ESCO2 is to catalyze SMC3 acetylation (SMC3ac) during cohesion establishment, we then assessed whether GSK3s affect this reaction. We measured the SMC3ac levels by probing with an antibody specific to SMC3ac. Since SMC3 is acetylated and deacetylated in a cell-cycle-regulated pattern (41,42), we next synchronized 293T cells in early S phase by double-thymidine blocks and carried out time-course measurements of the Smc3ac levels. After the addition of GSK3i for half an hour, cells were released into fresh media containing nocodazole to arrest in metaphase. Samples were harvested every hour. Chromatin fractions were prepared and chromatin-associated proteins were analyzed by immunoblotting (Figure 4A). As shown in flow cytometry, the cell cycle progression was only slightly affected by GSK3 inhibition (Supplementary Figure S4A–C). The overall levels of MMS22L in whole-cell lysates remained constant. However, the chromatin-bound levels of MMS22L displayed a cell-cycle-oscillated pattern, correlating well with those of ESCO2 and SMC3ac (Figure 4B and C). Intriguingly, GSK3i treatment caused a moderate delay in the accumulation of MMS22L, ESCO2 and SMC3ac on chromatin in both 293T (Figure 4B and C) and HepG2 cells (Supplementary Figure S5A–C). These results suggest that the ESCO2-regulatory role of MMS22L largely depends on GSK3s.

The GSK3s-CRL4^{MMS22L}-ESCO2 model predicts that enforcing ESCO2 dimerization will bypass the requirement of GSK3s in cohesion establishment. To explore this possibility, we compared the effects of various tags to the Eco1 C-terminus on sister chromatid cohesion in budding yeast. Importantly, GFP and GST, well-known for their homo-dimerization capabilities, were able to efficiently rescue the cohesion defects due to a lack of *MCK1* (Supplementary Figure S4D). On the contrary, a monomeric GFP variant (mGFP, also used in Figure 3H) exacerbated the cohesion loss in *mck1*Δ cells. Intriguingly, mGFP alone caused a prominent cohesion defect even in WT cells. These imply that Eco1 carrying a dimeric tag (GFP and GST) is sufficient to replace the cohesion function of Mck1. To confirm this result, we adopted a rapamycin-inducible dimerization system. To avoid overexpression of Eco1, we performed the cohesion analysis in the diploid yeast cells with two endogenous copies of Eco1 harboring FRB and FKBP tags, respectively. As shown in Figure 4D and Supplementary Figure S4E, only a complete set of rapamycin-inducible dimerization of Eco1 can fully rescue the cohesion loss in *mck1*Δ/*mck1*Δ cells. There were no effects when either an FKBP tag or rapamycin was omitted (Figure 4D and Supplementary Figure S4E). These data together suggest the cohesion role of Mck1 is solely attributed to Eco1 dimerization.

In sum, we propose that GSK3s phosphorylate and dimerize CRL4^{MMS22L}, which subsequently leads to the simultaneous recruitment of two ESCO2 molecules and thus provides stringent quality control of the vital cohesion establishment reaction (Figure 5).

DISCUSSION

Besides SMC3, Eco1 or ESCO2 is able to acetylate other substrates including PCNA (43). During cohesion establishment, how it is specifically targeted to a subset of cohesin entrapping sister chromatids remains an open question. In this study, we show that ESCO2 might be under hierarchical control via the GSK3-mediated CRL4^{MMS22L} homo-dimerization to achieve highly accurate targeting cohesin exclusively in the context of sister chromatids. This finding indicates that GSK3 family kinases also define a stringent quality control of cohesion establishment and chromosome integrity, in addition to their best-known functions in glucose metabolism, cell proliferation, apoptosis, embryonic development and neuronal signaling (32,44–46).

It is unanticipated that GSK3s enhance chromatin association of ESCO2 through CRL4^{MMS22L} homo-dimerization because GSK3 (Mck1) triggers Eco1 degra-

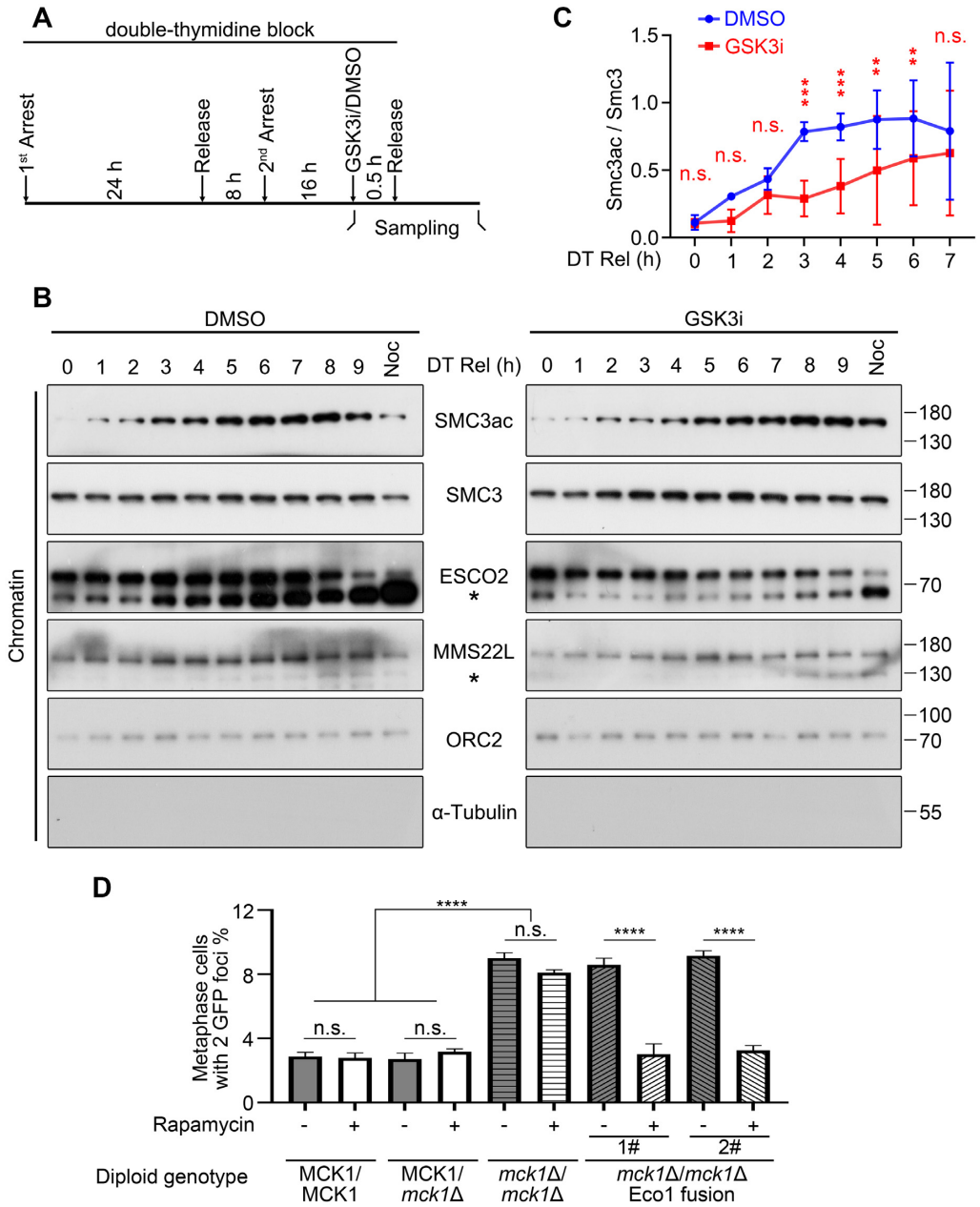

Figure 4. GSK3s promote the chromatin association of ESCO2 and SMC3 acetylation in S phase. (**A**) The outline of time-course experiments. The cells were synchronized using double-thymidine blocks. DMSO/GSK3 inhibitor was added half an hour before release. 5 h after release from the second thymidine block, nocodazole (Noc) was applied. Cell samples were harvested at different time points after DT Rel. (**B**) Chromatin fractions were prepared from 293T cells harvested as described above and analyzed by western blotting with the indicated antibodies. ORC2 served as a loading control of the chromatin-associated protein. (**C**) Quantification of SMC3 acetylation level in S phase (0–7 h after DT Rel). Band intensities in (B) were quantified by Quantity One software. The relative SMC3ac/SMC3 ratio was calculated. The statistical significance was analyzed via two-way ANOVA. The data represent mean ± SEM, $^{**}P > 0.01$, $^{***}P > 0.001$. (**D**) Artificial dimerization of Eco1 rescues the cohesion defect caused by *MCK1* deletion. Diploid yeast strains with the indicated genotypes (SBY214 background) were grown to log phase and sequentially synchronized with nocodazole in metaphase. Dimerization of Eco1 carrying FRB and FKBP tags was induced by adding rapamycin. At least 200 metaphase-arrested cells were counted for each experiment. Means ± SEM are shown. The statistical significance was calculated via one-way ANOVA, $^{****}P < 0.0001$.

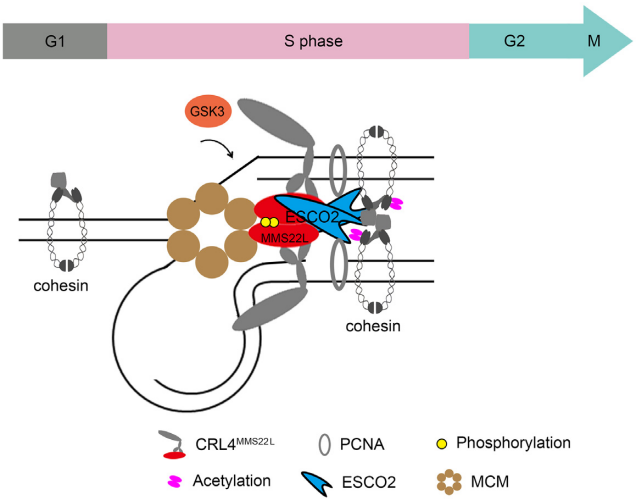

Figure 5. A proposed symmetric establishment model of sister chromatid cohesion in eukaryotes. During S phase, GSK3s phosphorylate MMS22L and trigger $CRL4^{MMS22L}$ dimerization, which presents dimeric ESCO2 for efficient SMC3 acetylation, the key reaction to establish cohesion between nascent sister chromatids.

dation in late S and G2 phases in budding yeast (47,48). Whether ESCO2 is degraded by a similar mechanism in humans remains to be answered, however, it is worth noting that it is not surprising if GSK3s have two opposing roles in ESCO2 regulation in the cohesion-dissolution cycle. Seoane and Morgan demonstrate that, in late S phase, Dbf4-dependent kinase (DDK) is released from its obligated substrate, the core replicative helicase MCM, so that it can phosphorylate Eco1. Eco1 is in turn primed for Mck1 kinase, and these sequential phosphorylation modifications eventually create a degron recognized by the ubiquitin ligase SCF^{Cdc4} (49). It will also be of interest to identify the kinase for priming MMS22L phosphorylation by GSK3s during S phase in the future.

Although dimerization is frequently employed in a large number of CRLs including $CRL4^{DDB2}$ and $CRL4^{DCAF}$ (50–52), GSK3-mediated $CRL4^{MMS22L}$ homo-dimerization provides unanticipated implications to the high specificity of ESCO2 and quality control of cohesion establishment.

The single-ring model, i.e. one cohesin encircles twin sisters, is proposed primarily based on studies showing that no self-interaction between the cohesin subunit is detected in yeast (53–56). These negative results are due to the affinity tag at the C-terminus of SCC1 used for detecting self-interaction. Through a simple switch to the N-terminal tagging, Pati's group and our group independently report the cohesin-cohesin interaction in an antiparallel manner in human and yeast cells (39,57). The intermolecular interaction of cohesin is also supported by genetic and biochemical evidence from many groups (58–61). Recently, we show that cohesin is dimerized during S phase in a DNA replication-coupled and Eco1-dependent manner (39). Dimeric cohesin contains two SMC3, requiring either two ESCO2 molecules to acetylate simultaneously or one enzyme to operate successively. The latter scenario is evidently less efficiency and more error-prone, which does not meet the high-fidelity demand of sister chromatid cohesion. This notion is also supported by the apparent cohesion defects observed in the MMS22L phosphorylation/dimerization mutant or when GSK3s are inhibited. Furthermore, balanced retention of PCNA, another crucial Eco1 regulator, on both leading and lagging strands has recently been shown to promote Smc3 acetylation, although PCNA seems dispensable for leading strand DNA synthesis. In this study, we have shown that although Eco1 exists as a monomer by itself, Eco1/ESCO2 is homo-dimerized through GSK3-mediated $CRL4^{MMS22L}$ dimerization during S phase in yeast and humans. Therefore, we postulate that dimeric $CRL4^{MMS22L}$, cooperatively with balanced PCNA on leading and lagging strands, may provide docking sites for two ESCO2 molecules, which can simultaneously catalyze two SMC3 in two single-ring cohesin complexes to establish a double-ring cohesion state. Although they are not necessarily mutually exclusive, the symmetric 'double-enzyme double-ring' model may have several advantages over the 'single-enzyme single-ring' one. For example, it can cause an exponential decline in the off-target rate compared with a single 'leaky' reaction of ESCO2. Cohesion would not occur even when single-ring cohesin is encountered and acetylated by ESCO2. It can only occur in the context of ongoing replication forks, which have a two-fold axis of symmetry, thereby providing more stringent quality control to preclude false cohesion between non-sister chromatids. Nevertheless, we have to acknowledge that this model is still speculative at the current stage; more direct evidence such as the high-resolution structure of a double-ring cohesin complex will be needed in the future.

DATA AVAILABILITY

The data underlying this article are included in the online Supplementary Data file or available from the corresponding author upon reasonable request.

SUPPLEMENTARY DATA

Supplementary Data are available at NAR Online.

ACKNOWLEDGEMENTS

We're grateful to Drs Sue Biggins (Fred Hutchinson Cancer Research Center, USA), Katsuhiko Shirahige (University of Tokyo) and Jun Tang (China Agricultural University, China) for generously sharing materials, Dr. Robert V. Skibbens (Lehigh University, USA) for valuable suggestions and comments on the manuscript, members of the Lou laboratory for discussion. We thank Instrumental Analysis Center of Shenzhen University for the assistance with fluorescence imaging analysis.
Author contributions: Huiqiang Lou and Jiaxin Zhang conceived and designed the overall project; Jiaxin Zhang and Lili Li conducted most experiments with the help from other authors; Chunlai Chen and Yu Miao designed and performed FCS/PCD experiments and computation; Xiaojing Liu, Haitao Sun, Meiqian Jiang, Xiaoli Li, Wenya Hou and Cong Liu prepared some materials; Zhen Li performed mass spectrometry; Huiqiang Lou and Jiaxin Zhang wrote the manuscript with inputs and editing from all of the authors.

FUNDING

National Natural Science Foundation of China [32161133015 to H.L., 32101039 to W.H.]; National Key R&D Program of China [2019YFA0903900 to H.L.]; National Natural Science Foundation of China [21877069, 21922704, 22061160466 to C.C.]; Beijing Municipal Natural Science Foundation [5212010 to Q.C.]; Natural science foundation of Guangdong province of China [2022A1515012495 to H.L., 2022A1515011208 to W.H.]; China Postdoctoral Science Foundation [2022T150435 to L.L.]; SZU Top Ranking Project [86000000210 to H.L.]. Funding for open access charge: National Natural Science Foundation of China.

Conflict of interest statement. None declared.

REFERENCES

1. Peters,J.M. and Nishiyama,T. (2012) Sister chromatid cohesion. *Cold Spring Harb. Perspect. Biol.*, **4**, a011130.
2. Zheng,G. and Yu,H. (2015) Regulation of sister chromatid cohesion during the mitotic cell cycle. *Sci China Life Sci*, **58**, 1089–1098.
3. Nasmyth,K. and Haering,C.H. (2009) Cohesin: its roles and mechanisms. *Annu. Rev. Genet.*, **43**, 525–558.
4. Morales,C. and Losada,A. (2018) Establishing and dissolving cohesion during the vertebrate cell cycle. *Curr. Opin. Cell Biol.*, **52**, 51–57.
5. Kim,Y. and Yu,H. (2020) Shaping of the 3D genome by the ATPase machine cohesin. *Exp. Mol. Med.*, **52**, 1891–1897.
6. Yatskevich,S., Rhodes,J. and Nasmyth,K. (2019) Organization of chromosomal DNA by SMC complexes. *Annu. Rev. Genet.*, **53**, 445–482.
7. Gandhi,R., Gillespie,P.J. and Hirano,T. (2006) Human Wapl is a cohesin-binding protein that promotes sister-chromatid resolution in mitotic prophase. *Curr. Biol.*, **16**, 2406–2417.
8. Losada,A., Yokochi,T. and Hirano,T. (2005) Functional contribution of Pds5 to cohesin-mediated cohesion in human cells and Xenopus egg extracts. *J. Cell Sci.*, **118**, 2133–2141.
9. Nishiyama,T., Ladurner,R., Schmitz,J., Kreidl,E., Schleiffer,A., Bhaskara,V., Bando,M., Shirahige,K., Hyman,A.A., Mechtler,K. *et al.* (2010) Sororin mediates sister chromatid cohesion by antagonizing Wapl. *Cell*, **143**, 737–749.
10. Xiong,B. and Gerton,J.L. (2010) Regulators of the cohesin network. *Annu. Rev. Biochem.*, **79**, 131–153.
11. Hou,F. and Zou,H. (2005) Two human orthologues of Eco1/Ctf7 acetyltransferases are both required for proper sister-chromatid cohesion. *Mol. Biol. Cell*, **16**, 3908–3918.
12. Rolef Ben-Shahar,T., Heeger,S., Lehane,C., East,P., Flynn,H., Skehel,M. and Uhlmann,F. (2008) Eco1-dependent cohesin acetylation during establishment of sister chromatid cohesion. *Science*, **321**, 563–566.
13. Ivanov,D., Schleiffer,A., Eisenhaber,F., Mechtler,K., Haering,C.H. and Nasmyth,K. (2002) Eco1 is a novel acetyltransferase that can acetylate proteins involved in cohesion. *Curr. Biol.*, **12**, 323–328.
14. Unal,E., Heidinger-Pauli,J.M., Kim,W., Guacci,V., Onn,I., Gygi,S.P. and Koshland,D.E. (2008) A molecular determinant for the establishment of sister chromatid cohesion. *Science*, **321**, 566–569.
15. Zhang,J., Shi,X., Li,Y., Kim,B.J., Jia,J., Huang,Z., Yang,T., Fu,X., Jung,S.Y., Wang,Y. *et al.* (2008) Acetylation of Smc3 by Eco1 is required for S phase sister chromatid cohesion in both human and yeast. *Mol. Cell*, **31**, 143–151.
16. Lengronne,A., Katou,Y., Mori,S., Yokobayashi,S., Kelly,G.P., Itoh,T., Watanabe,Y., Shirahige,K. and Uhlmann,F. (2004) Cohesin relocation from sites of chromosomal loading to places of convergent transcription. *Nature*, **430**, 573–578.
17. Moldovan,G.L., Pfander,B. and Jentsch,S. (2006) PCNA controls establishment of sister chromatid cohesion during S phase. *Mol. Cell*, **23**, 723–732.
18. Song,J., Lafont,A., Chen,J., Wu,F.M., Shirahige,K. and Rankin,S. (2012) Cohesin acetylation promotes sister chromatid cohesion only in association with the replication machinery. *J. Biol. Chem.*, **287**, 34325–34336.
19. Sherwood,R., Takahashi,T.S. and Jallepalli,P.V. (2010) Sister acts: coordinating DNA replication and cohesion establishment. *Genes Dev.*, **24**, 2723–2731.
20. Borges,V., Smith,D.J., Whitehouse,I. and Uhlmann,F. (2013) An Eco1-independent sister chromatid cohesion establishment pathway in S. cerevisiae. *Chromosoma*, **122**, 121–134.
21. Skibbens,R.V., Corson,L.B., Koshland,D. and Hieter,P. (1999) Ctf7p is essential for sister chromatid cohesion and links mitotic chromosome structure to the DNA replication machinery. *Genes Dev.*, **13**, 307–319.
22. Sun,H., Zhang,J., Xin,S., Jiang,M., Zhang,J., Li,Z., Cao,Q. and Lou,H. (2019) Cul4-Ddb1 ubiquitin ligases facilitate DNA replication-coupled sister chromatid cohesion through regulation of cohesin acetyltransferase Esco2. *PLoS Genet.*, **15**, e1007685.
23. Zhang,J., Shi,D., Li,X., Ding,L., Tang,J., Liu,C., Shirahige,K., Cao,Q. and Lou,H. (2017) Rtt101-Mms1-Mms22 coordinates replication-coupled sister chromatid cohesion and nucleosome assembly. *EMBO Rep.*, **18**, 1294–1305.
24. Cong,L., Ran,F.A., Cox,D., Lin,S., Barretto,R., Habib,N., Hsu,P.D., Wu,X., Jiang,W., Marraffini,L.A. *et al.* (2013) Multiplex genome engineering using CRISPR/Cas systems. *Science*, **339**, 819–823.
25. Minamino,M., Ishibashi,M., Nakato,R., Akiyama,K., Tanaka,H., Kato,Y., Negishi,L., Hirota,T., Sutani,T., Bando,M. *et al.* (2015) Esco1 acetylates cohesin via a mechanism different from that of Esco2. *Curr. Biol.*, **25**, 1694–1706.
26. Thaminy,S., Newcomb,B., Kim,J., Gatbonton,T., Foss,E., Simon,J. and Bedalov,A. (2007) Hst3 is regulated by Mec1-dependent proteolysis and controls the S phase checkpoint and sister chromatid cohesion by deacetylating histone H3 at lysine 56. *J. Biol. Chem.*, **282**, 37805–37814.
27. Nishitani,H., Morino,M., Murakami,Y., Maeda,T. and Shiomi,Y. (2014) Chromatin fractionation analysis of licensing factors in mammalian cells. *Methods Mol. Biol.*, **1170**, 517–527.
28. Ha,T., Rasnik,I., Cheng,W., Babcock,H.P., Gauss,G.H., Lohman,T.M. and Chu,S. (2002) Initiation and re-initiation of DNA unwinding by the Escherichia coli Rep helicase. *Nature*, **419**, 638–641.
29. Peng,S., Sun,R., Wang,W. and Chen,C. (2017) Single-molecule photoactivation FRET: a general and easy-to-implement approach to break the concentration barrier. *Angew. Chem. Int. Ed Engl.*, **56**, 6882–6885.
30. Skakun,V.V., Engel,R., Digris,A.V., Borst,J.W. and Visser,A. (2011) Global analysis of autocorrelation functions and photon counting distributions. *Front. Biosci. (Elite Ed.)*, **3**, 489–505.
31. MacAulay,K., Doble,B.W., Patel,S., Hansotia,T., Sinclair,E.M., Drucker,D.J., Nagy,A. and Woodgett,J.R. (2007) Glycogen synthase kinase 3alpha-specific regulation of murine hepatic glycogen metabolism. *Cell Metab.*, **6**, 329–337.
32. Hoeflich,K.P., Luo,J., Rubie,E.A., Tsao,M.S., Jin,O. and Woodgett,J.R. (2000) Requirement for glycogen synthase kinase-3beta in cell survival and NF-kappaB activation. *Nature*, **406**, 86–90.
33. McQueen,J., van Dyk,D., Young,B., Loewen,C. and Measday,V. (2012) The Mck1 GSK-3 kinase inhibits the activity of Clb2-Cdk1 post-nuclear division. *Cell Cycle*, **11**, 3421–3432.
34. Lee,J., Moir,R.D., McIntosh,K.B. and Willis,I.M. (2012) TOR signaling regulates ribosome and tRNA synthesis via LAMMER/Clk and GSK-3 family kinases. *Mol. Cell*, **45**, 836–843.
35. Nicot,A.S., Lo Verso,F., Ratti,F., Pilot-Storck,F., Streichenberger,N., Sandri,M., Schaeffer,L. and Goillot,E. (2014) Phosphorylation of NBR1 by GSK3 modulates protein aggregation. *Autophagy*, **10**, 1036–1053.
36. Cohen,P. and Frame,S. (2001) The renaissance of GSK3. *Nat. Rev. Mol. Cell Biol.*, **2**, 769–776.
37. Onn,I., Guacci,V. and Koshland,D.E. (2009) The zinc finger of Eco1 enhances its acetyltransferase activity during sister chromatid cohesion. *Nucleic Acids Res.*, **37**, 6126–6134.
38. Kouznetsova,E., Kanno,T., Karlberg,T., Thorsell,A.G., Wisniewska,M., Kursula,P., Sjögren,C. and Schüler,H. (2016) Sister chromatid cohesion establishment factor ESCO1 operates by substrate-assisted catalysis. *Structure*, **24**, 789–796.

39. Shi,D., Zhao,S., Zuo,M.Q., Zhang,J., Hou,W., Dong,M.Q., Cao,Q. and Lou,H. (2020) The acetyltransferase Eco1 elicits cohesin dimerization during S phase. *J. Biol. Chem.*, **295**, 7554–7565.
40. Nederveen-Schippers,L.M., Pathak,P., Keizer-Gunnink,I., Westphal,A.H., van Haastert,P.J., Borst,J.W., Kortholt,A. and Skakun,V. (2021) Combined fcs and pch analysis to quantify protein dimerization in living cells. *Int. J. Mol. Sci.*, **22**, 7300.
41. Beckouët,F., Hu,B., Roig,M.B., Sutani,T., Komata,M., Uluocak,P., Katis,V.L., Shirahige,K. and Nasmyth,K. (2010) An Smc3 acetylation cycle is essential for establishment of sister chromatid cohesion. *Mol. Cell*, **39**, 689–699.
42. Borges,V., Lehane,C., Lopez-Serra,L., Flynn,H., Skehel,M., Rolef Ben-Shahar,T. and Uhlmann,F. (2010) Hos1 deacetylates Smc3 to close the cohesin acetylation cycle. *Mol. Cell*, **39**, 677–688.
43. Billon,P., Li,J., Lambert,J.P., Chen,Y., Tremblay,V., Brunzelle,J.S., Gingras,A.C., Verreault,A., Sugiyama,T., Couture,J.F. *et al.* (2017) Acetylation of PCNA sliding surface by Eco1 promotes genome stability through homologous recombination. *Mol. Cell*, **65**, 78–90.
44. Beurel,E., Grieco,S.F. and Jope,R.S. (2015) Glycogen synthase kinase-3 (GSK3): regulation, actions, and diseases. *Pharmacol. Ther.*, **148**, 114–131.
45. Baehr,C.A., Huntoon,C.J., Hoang,S.M., Jerde,C.R. and Karnitz,L.M. (2016) Glycogen synthase kinase 3 (GSK-3)-mediated phosphorylation of uracil N-glycosylase 2 (UNG2) facilitates the repair of floxuridine-induced DNA lesions and promotes cell survival. *J. Biol. Chem.*, **291**, 26875–26885.
46. Yang,Y., Lei,T., Du,S., Tong,R., Wang,H., Yang,J., Huang,J., Sun,M., Wang,Y. and Dong,Z. (2018) Nuclear GSK3β induces DNA double-strand break repair by phosphorylating 53BP1 in glioblastoma. *Int. J. Oncol.*, **52**, 709–720.
47. Seoane,A.I. and Morgan,D.O. (2017) Firing of replication origins frees Dbf4-Cdc7 to target Eco1 for destruction. *Curr. Biol.*, **27**, 2849–2855.
48. Lyons,N.A., Fonslow,B.R., Diedrich,J.K., Yates,J.R. 3rd and Morgan,D.O. (2013) Sequential primed kinases create a damage-responsive phosphodegron on Eco1. *Nat. Struct. Mol. Biol.*, **20**, 194–201.
49. Lyons,N.A. and Morgan,D.O. (2011) Cdk1-dependent destruction of Eco1 prevents cohesion establishment after S phase. *Mol. Cell*, **42**, 378–389.
50. Ahn,J., Novince,Z., Concel,J., Byeon,C.H., Makhov,A.M., Byeon,I.J., Zhang,P. and Gronenborn,A.M. (2011) The Cullin-RING E3 ubiquitin ligase CRL4-DCAF1 complex dimerizes via a short helical region in DCAF1. *Biochemistry*, **50**, 1359–1367.
51. Merlet,J., Burger,J., Gomes,J.E. and Pintard,L. (2009) Regulation of cullin-RING E3 ubiquitin-ligases by neddylation and dimerization. *Cell. Mol. Life Sci.*, **66**, 1924–1938.
52. Yeh,J.I., Levine,A.S., Du,S., Chinte,U., Ghodke,H., Wang,H., Shi,H., Hsieh,C.L., Conway,J.F., Van Houten,B. *et al.* (2012) Damaged DNA induced UV-damaged DNA-binding protein (UV-DDB) dimerization and its roles in chromatinized DNA repair. *Proc. Natl. Acad. Sci. U.S.A.*, **109**, E2737–E2746.
53. Haering,C.H., Löwe,J., Hochwagen,A. and Nasmyth,K. (2002) Molecular architecture of SMC proteins and the yeast cohesin complex. *Mol. Cell*, **9**, 773–788.
54. Mc Intyre,J., Muller,E.G., Weitzer,S., Snydsman,B.E., Davis,T.N. and Uhlmann,F. (2007) In vivo analysis of cohesin architecture using FRET in the budding yeast Saccharomyces cerevisiae. *EMBO J.*, **26**, 3783–3793.
55. Gruber,S., Haering,C.H. and Nasmyth,K. (2003) Chromosomal cohesin forms a ring. *Cell*, **112**, 765–777.
56. Liu,W., Biton,E., Pathania,A., Matityahu,A., Irudayaraj,J. and Onn,I. (2020) Monomeric cohesin state revealed by live-cell single-molecule spectroscopy. *EMBO Rep.*, **21**, e48211.
57. Zhang,N., Kuznetsov,S.G., Sharan,S.K., Li,K., Rao,P.H. and Pati,D. (2008) A handcuff model for the cohesin complex. *J. Cell Biol.*, **183**, 1019–1031.
58. Eng,T., Guacci,V. and Koshland,D. (2015) Interallelic complementation provides functional evidence for cohesin-cohesin interactions on DNA. *Mol. Biol. Cell*, **26**, 4224–4235.
59. Kulemzina,I., Schumacher,M.R., Verma,V., Reiter,J., Metzler,J., Failla,A.V., Lanz,C., Sreedharan,V.T., Rätsch,G. and Ivanov,D. (2012) Cohesin rings devoid of Scc3 and Pds5 maintain their stable association with the DNA. *PLoS Genet.*, **8**, e1002856.
60. Tong,K. and Skibbens,R.V. (2014) Cohesin without cohesion: a novel role for Pds5 in *Saccharomyces cerevisiae*. *PLoS One*, **9**, e100470.
61. Matityahu,A. and Onn,I. (2022) It's all in the numbers: cohesin stoichiometry. *Front. Mol. Biosci.*, **9**, 1010894.